ELSEVIER

Biochimica et Biophysica Acta 1459 (2000) 248–257

BIOCHIMICA ET BIOPHYSICA ACTA
BBA

www.elsevier.com/locate/bba

Solution structure of the NADP(H)-binding component (dIII) of proton-translocating transhydrogenase from *Rhodospirillum rubrum*

Mark Jeeves, K. John Smith [1], Philip G. Quirk, Nick P.J. Cotton, J. Baz. Jackson *

School of Biosciences, University of Birmingham, Edgbaston, Birmingham, B15 2TT, UK

Received 12 April 2000; received in revised form 12 June 2000; accepted 12 June 2000

Abstract

Transhydrogenase is a proton pump found in the membranes of bacteria and animal mitochondria. The solution structure of the expressed, 21.5 kDa, NADP(H)-binding component (dIII) of transhydrogenase from *Rhodospirillum rubrum* has been solved by NMR methods. This is the first description of the structure of dIII from a bacterial source. The protein adopts a Rossmann fold: an open, twisted, parallel β-sheet, flanked by helices. However, the binding of $NADP^+$ to dIII is profoundly different to that seen in other Rossmann structures, in that its orientation is reversed: the adenosine moiety interacts with the first βαβαβ motif, and the nicotinamide with the second. Features in the structure that might be responsible for changes in nucleotide-binding affinity during catalysis, and for interaction with other components of the enzyme, are identified. The results are compared with the recently determined, high-resolution crystal structures of human and bovine dIII which also show the reversed nucleotide orientation.

Keywords: Transhydrogenase; Membrane protein; Proton translocation; Nuclear magnetic resonance structure; Nucleotide binding

1. Introduction

Transhydrogenase couples the transfer of reducing equivalents (hydride-ion equivalents) between NAD(H) and NADP(H) to the translocation of protons across a membrane (for review, see [1]):

$$H^+_{out} + NADH + NADP^+ \Leftrightarrow H^+_{in} + NAD^+ + NADPH \quad (1)$$

The enzyme is located in the inner mitochondrial membrane of animal cells, and in the cytoplasmic membrane of some species of bacteria. Usually, the reaction is driven from left to right by the proton electrochemical gradient (Δp) generated by respiratory (or photosynthetic) electron transfer. In bacteria, transhydrogenase provides NADPH for biosynthesis [2], but in mammalian mitochondria its function is probably to control flux though the tricarboxylic acid cycle [3].

Transhydrogenase consists of three components:

Abbreviations: dI, NAD(H)-binding portion of transhydrogenase; dII, membrane-embedded portion; dIII, NADP(H)-binding portion; HSQC, heteronuclear single-quantum coherence; NOE, Nuclear Overhauser Effect; NOESY, Nuclear Overhauser Effect spectroscopy; $AcPdAD^+$, acetyl pyridine adenine dinucleotide (oxidised form); TOCSY, total correlation spectroscopy; HCCH, ^1H-^{13}C-^{13}C-^1H correlation; COSY, correlation spectroscopy; t_m, mixing time; HMQC, heteronuclear multiple-quantum coherence

* Corresponding author. Fax: +44 (121) 4143982; E-mail: j.b.jackson@bham.ac.uk

[1] Present address: School of Biological Sciences, University of Southampton, Southampton, SO16 7PX, UK.

0005-2728/00/$ – see front matter
PII: S0005-2728(00)00159-6

an NAD(H)-binding portion (designated dI), a hydrophobic, membrane-embedded portion (dII), and an NADP(H)-binding portion (dIII). Both dI and dIII protrude from the same side of the membrane (the cytoplasmic side in bacteria). In mammalian mitochondria, transhydrogenase comprises a single polypeptide; in bacteria the enzyme is composed of two or three polypeptides. However, gene sequences indicate that, unlike other proteins of oxidative phosphorylation, transhydrogenases in mitochondria and bacteria have a similar subunit organisation. Soluble, recombinant forms of dI and dIII have been expressed using the cloned genes from *Rhodospirillum rubrum* [4,5], *Escherichia coli* [6], beef heart [7] and human heart [8]. Recombinant dI specifically binds NAD^+/NADH, and recombinant dIII specifically binds $NADP^+$/NADPH. A mixture of dI and dIII (from the same or even from different species) forms a complex which catalyses rapid hydride transfer between NAD(H) and NADP(H) or their analogues [5–8]. The rate of reaction catalysed by the dI:dIII complex is limited by slow dissociation of nucleotide from dIII [5].

In complete transhydrogenase, Δp is believed to drive the reaction by modulating the binding affinities of the enzyme for $NADP^+$ and NADPH [9,10]. Although hydride transfer in the dI:dIII complex is well characterised (e.g. [11,12]), our knowledge of the associated conformational events and the mechanism by which these are coupled to proton translocation has been severely limited by the lack of available structure information. High resolution crystal structures of the dIII protein from bovine [13] and human [1,14] mitochondria were recently described. Secondary structure predictions of bacterial dIII (from *R. rubrum* [15] and *E. coli* [16]) based on NMR analysis were generally consistent with the crystal structures of the mammalian proteins. However, there were apparent differences between the preliminary 'global fold' of *E. coli* dIII (*ec*dIII) obtained from NMR data [16], and the crystallographically determined fold of the bovine and human proteins. Here, we present the solution structure of the $NADP^+$-bound form of dIII from *R. rubrum* transhydrogenase (*rr*dIII). The fold of the protein and its mode of nucleotide binding are compared with those in the mammalian dIII structures. Knowledge of the solution structure of *rr*dIII allows an improved interpretation of our earlier NMR studies of the interactions of the protein with dI, and of the effect of the redox state of the bound nucleotide on the protein conformation [15].

2. Experimental procedures

2.1. Sample preparation

Recombinant *rr*dIII, in either unlabelled, ^{15}N-labelled, or ^{13}C, ^{15}N-labelled forms, was expressed in *E. coli* BL21(DE3) from the plasmid pNIC2 and purified by column chromatography [5,17]. It contained approx. 1 mole of tightly bound NADP(H) per mole of protein. This nucleotide was not isotopically labelled in the labelled protein preparations, due to exchange with the 2 μM $NADP^+$ present in all the column and dialysis buffers. To ensure sample homogeneity, *rr*dIII was incubated with $AcPdAD^+$ and dI in order to oxidise any bound NADPH to $NADP^+$, and then re-purified [17]. Samples of between 500 and 800 μM protein were prepared in buffer containing 20 mM HEPES (pH 7.2), 2 μM $NADP^+$, 50 μM 4-(2-aminoethyl)benzenesulphonyl fluoride (AEBSF), 0.1% (w/v) sodium azide and 50 μg/ml chloramphenicol. These concentrations of azide, AEBSF and chloramphenicol did not affect the catalytic activity of the protein. The solvent was 92% H_2O/8% ^2H_2O or 99.9% ^2H_2O, as required. In all cases, pH values were taken from the meter readings, without correction for the deuterium isotope effect. Samples were filter sterilised using a 0.22 μm filter (Millipore) immediately prior to addition to the NMR tube.

2.2. General NMR parameters

All NMR experiments were performed on a Varian UnityPlus spectrometer, operating at 599.983 MHz for ^1H, except for the HNHB, which was performed on a Bruker AMX spectrometer operating at 500.13 MHz for ^1H. Quadrature detection was achieved using either the States time-proportional-phase-incrementation or sensitivity-enhanced protocols. All experiments were performed at 30°C. Spectra were transformed using Vnmr (Varian) software for the 3D spectra and UXNMR (Bruker) software for the 2D spectra. Peaks were picked using

NMRCompass (MSI). Chemical shifts were referenced indirectly to external tetramethylsilane. ^{1}H, ^{15}N HSQC spectra were acquired before and after each experiment to ensure that the protein had not degraded while in the spectrometer.

2.3. Assignment of resonances

The initial assignment of main chain $^{1}H^{N}$, ^{15}N, $^{13}C^{\alpha}$, $^{1}H^{\alpha}$, $^{13}C'$ and side chain $^{13}C^{\beta}$ resonances was described in [17]. Further side chain assignments were achieved using HNHB [18], CCH-TOCSY [19] with $t_m = 20$ ms, HC(C)H-COSY and (H)CCH-COSY [20] experiments. Stereospecific assignment was performed manually on the H^{β} protons, using the HNHB and HACAHB-COSY spectra [21]. The protons in the bound nucleotide were assigned using a ^{13}C, ^{15}N-double filtered, double-quantum filtered COSY experiment [22] in $^{2}H_2O$, ^{13}C, ^{15}N-double filtered NOESY experiments ($t_m = 50$, 100 and 300 ms) in H_2O and a ^{13}C, ^{15}N-double filtered NOESY experiment in $^{2}H_2O$ ($t_m = 300$ ms). These experiments utilised the filtering method of [23], with filtering applied both before and after the NOESY mixing time.

2.4. Calculation of torsion angles

Backbone ϕ and ψ dihedral angles were calculated from the chemical shift index, as given in [15]. Elimination of certain ranges of the side chain torsion angle (χ_1) was achieved from analysis of the HNHB and HACAHB-COSY spectra, and from the zero crossing point of a CT-HMQC experiment [24].

2.5. NOESY experiments

Protein-protein distance restraints were calculated from the following experiments: 2D ^{1}H-^{1}H NOESY ($t_m = 200$ ms) in $^{2}H_2O$; 3D ^{15}N-resolved NOESY-HSQC ($t_m = 200$ ms, 5 mm probe, solvent suppression by sensitivity enhancement) [25]; 3D ^{15}N-resolved NOESY-HSQC ($t_m = 200$ ms, 10 mm probe, solvent suppression by Watergate [26]); 3D ^{13}C-resolved NOESY-HMQC ($t_m = 300$ ms) and 3D ^{13}C-resolved HMQC-NOESY ($t_m = 300$ ms), both in $^{2}H_2O$ and $^{1}H_2O$, derived from [27]. Due to the rapid relaxation of magnetisation in *rr*dIII, both the 4D ^{13}C, ^{13}C-resolved HMQC-NOESY-HMQC [27] and the 4D ^{13}C, ^{15}N-resolved HMQC-NOESY-HSQC [28] (t_m values of 100–350 ms) spectra contained very few inter-residue peaks. Instead, we used the two 3D ^{13}C-resolved NOESY spectra, and cross-matched the two common dimensions to give a peak list equivalent to that from a 4D ^{13}C, ^{13}C-resolved experiment.

Distance restraints between protein and nucleotide were calculated primarily from a ^{13}C F_1-filtered, F_3-edited NOESY experiment ($t_m = 250$ ms) [23]. We also used the method of [23] to produce ^{13}C, ^{15}N F_1-filtered, ^{15}N-edited NOESY-HSQC and ^{13}C, ^{15}N F_1-filtered, ^{13}C-edited NOESY-HSQC spectra.

2.6. Calculation of structures

Over 200 intra-protein NOEs were assigned unambiguously from the pair of ^{13}C-resolved NOESY-HMQC and HMQC-NOESY spectra. These NOEs were used to generate a starting structure and the remaining NOEs were assigned, and distances calculated, using ARIA [29] in X-PLOR version 3.851

Table 1
Parameters for the family of *rr*dIII structures

(A) Experimental restraints	
NOEs	2257
Ambiguous	301
Unambiguous	1956
Intra-residue	890
Sequential ($d_{i,i+1}$)	410
Medium range ($d_{i,i+2}$ to $d_{i,i+4}$)	210
Long range ($d_{i,i+5}$ and greater)	446
Hydrogen bonds used in calculations	59
Dihedral restraints	
Backbone	173
χ_1	76
(B) Violations	
Average violation (all unambiguous NOEs)	0.022 Å
Violations ≥ 0.5 Å (max. 0.57 Å)	2
(C) RMSD (ten lowest energy structures)	
C^{α} only (residues 32–202)	1.01 Å
All atoms (residues 32–202)	1.69 Å
$NADP^{+}$ alone	1.39 Å
(D) Ramachandran plot (ten lowest energy structures)	
Most favoured	49.7%
Allowed	39.6%
Generously allowed	9.2%
Disallowed	1.4%

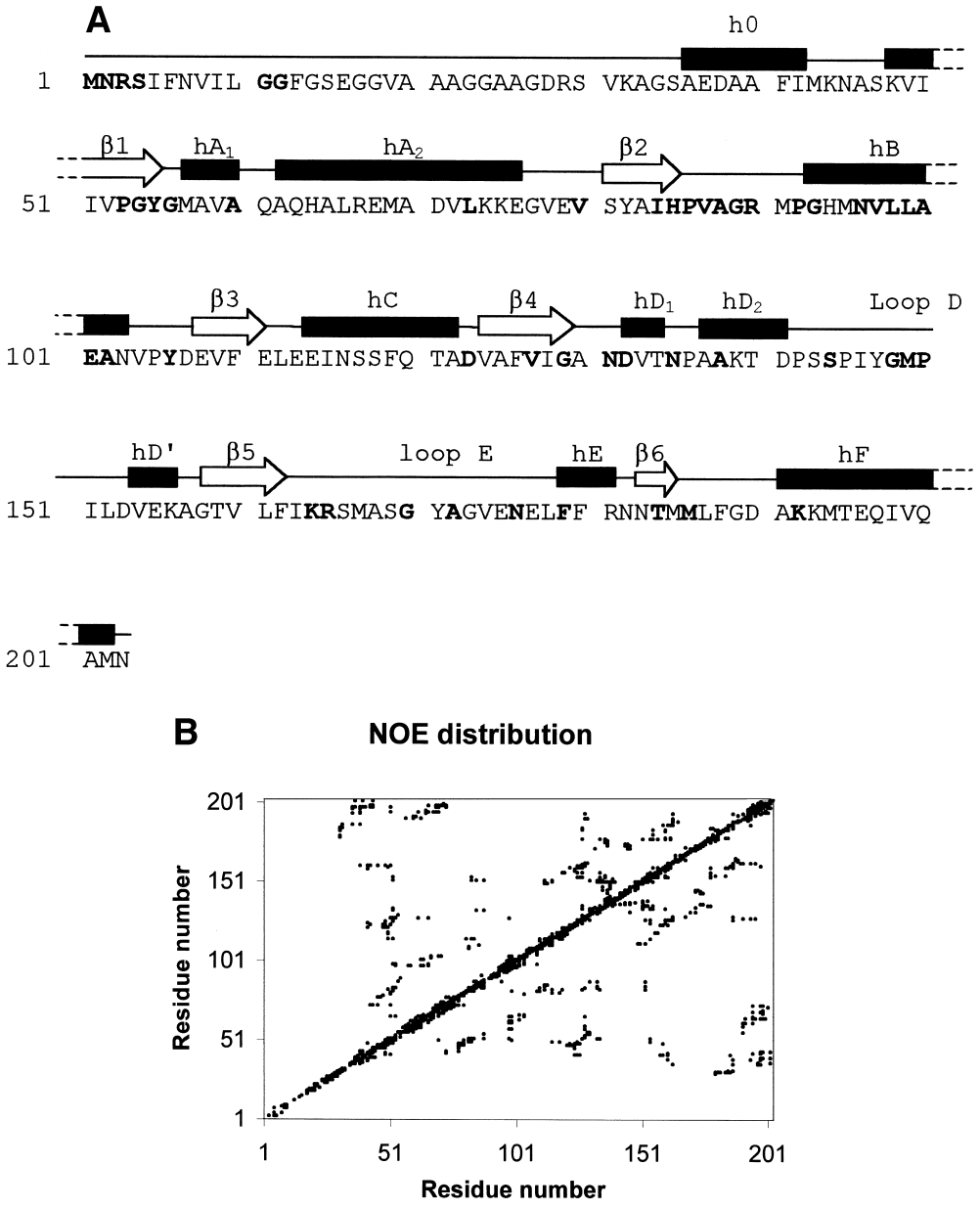

Fig. 1. (A) Sequence and secondary structure elements of *rr*dIII. h, helix; β, β-strand. Residues invariant in 11 other published sequences are shown in bold lettering. (B) Matrix representation of inter-residue NOE restraints, showing the distribution of long range NOEs.

[30]. Long-range d_{NN} and $d_{\alpha N}$ NOEs were identified from the NOESY-HSQC experiments performed on large samples of *rr*dIII (3.5 ml of 800 μM ^{15}N-labelled protein in the 10 mm probe). These together with the side chain to side chain NOEs were used to orient the β-strands relative to one another and to place each helix on the correct side of the β-sheet.

Restraints used in the final structural calculations are shown in Table 1, and the NOE distribution in Fig. 1B. In addition, a small number of very weak NOEs across the β-strands were identified, for which an upper distance limit of 7 Å was used in the structural calculations. Standard pseudoatom corrections were applied to the methyl protons. The ϕ and ψ angles for all assigned residues (except Gly, Asn and Pro) were restrained to the α-helix or β-sheet

regions of the Ramachandran plot on the basis of the chemical shift index [15]. Hydrogen bond donors were picked using the slowly exchanging amides noted previously [15]. Hydrogen bond acceptors were picked using preliminary structures in X-PLOR. In total, 59 hydrogen bonds were predicted, and restraints (two per hydrogen bond, where $r_{NH-O} = 1.8–2.2$ Å and $r_{N-O} = 2.2–3.3$ Å) were included in the final stages of refinement.

One hundred protein structures, in the absence of $NADP^+$, were determined in X-PLOR 3.851 [30], using a protocol in which certain atoms of each residue (C^α, H^α, N, H^N, C', and C^β, C^γ where present) were embedded using distance geometry. The remaining atoms were placed by template fitting, and then the atomic co-ordinates were allowed to evolve under the applied NOE distance and dihedral constraints during a series of high temperature annealing steps. The nucleotide and protein were docked using molecular dynamics, whilst holding the nucleotide rigid. Following energy minimisation, the structures were then subjected to three further iterations of simulated annealing. An average structure was calculated by simultaneously refining the ten lowest-energy structures in a high-temperature, simulated annealing protocol, and applying an additional constraint in order to minimise the root-mean-square difference between the aligned co-ordinates (non-crystalline symmetry restraints applied to all atoms of residues 29–202).

Analysis of the final ten lowest-energy structures was performed using the AQUA and PROCHECK-NMR packages [31]. Figures were generated using MOLSCRIPT [32].

3. Results and discussion

3.1. NMR resonance assignments and structure determinations

Assignments were previously obtained for all backbone resonances of *rr*dIII, apart from those from the first 14 amino acids, H^N and N of Tyr147 and the N signals from the eight proline residues [17]. In the current work, with the exception of the first 14 residues, the side chain ^1H and ^{13}C signals from Ala, Ser, Val, Thr, Leu, and Ile residues were assigned completely, along with all Asn/Asp to C^β-H^β, and all Gln/Glu to C^γ-H^γ. Problems arising from rapid relaxation and spectral overlap were encountered in the assignment of several Met C^γ-H^γ, Arg C^γ-H^γ and C^δ-H^δ, Pro C^γ-H^γ and C^δ-H^δ, and Lys C^δ-H^δ and C^ε-H^ε. Assignment of H^δ and H^ε was achieved for all 5 Tyr, and H^δ was assigned for six out of the ten Phe residues using the two-dimensional NOESY spectra in ^2H_2O (Phe 110, 119, 162, 179, 180, 188). All the non-exchangeable protons of the bound $NADP^+$ were assigned, with the exception of the adenine ribose H4′.

The data used to generate the family of solution structures are summarised in Table 1, together with relevant properties of the ten lowest energy structures. The co-ordinates of the averaged structure have been deposited in the Brookhaven PDB library (accession code 1e3t).

3.2. The protein fold

Recombinant dIII of *R. rubrum* contains 203 amino acid residues. It folds into a single, compact domain, of approx. 35 Å×35 Å×45 Å. Fig. 1 shows the protein sequence, the identified elements of secondary structure, and the distribution of inter-residue NOEs. The family of solution structures (Fig. 2) is well defined by the NOE-derived restraints. The overall structure (Fig. 3) has the common dinucleo-

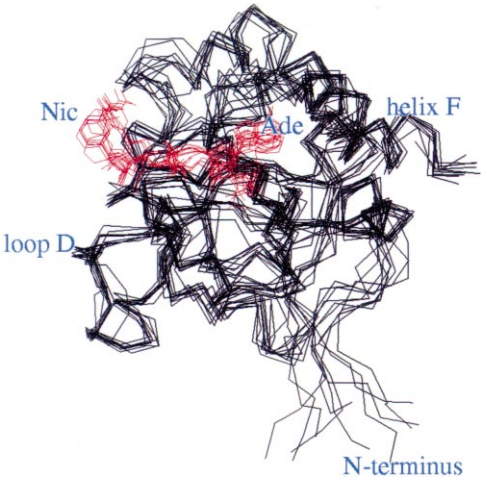

Fig. 2. Ensemble of the C^α traces (residues 26–203) of the ten lowest energy structures of *rr*dIII, aligned using the C^α atoms of residues 32–202. The bound $NADP^+$ of each structure is shown in red. The first 25 residues are highly disordered and are not shown.

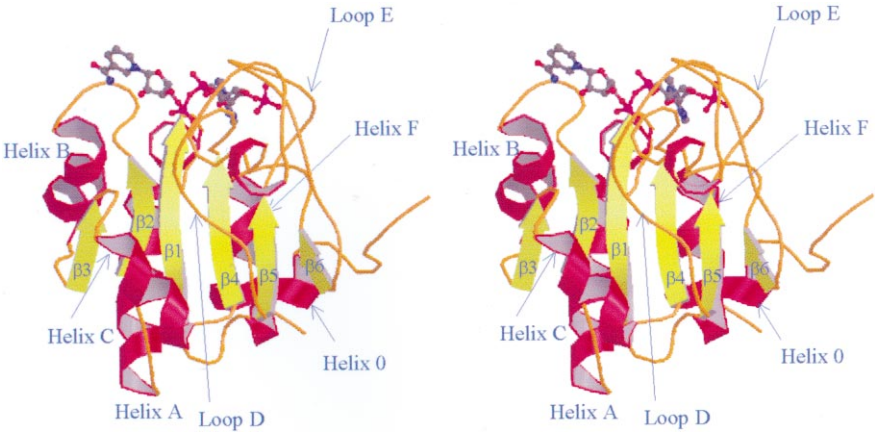

Fig. 3. Stereo cartoon of *rr*dIII fold. α-Helices (0, A–C, F; red) and β-strands (β1–β6; green) are superimposed on the backbone C^{α} trace of residues 29–203 of the averaged structure. Also labelled are loops D and E, but the single, weakly helical turns D_1, D′ and E are omitted for clarity. The bound $NADP^+$ is shown in ball-and-stick representation, with the nicotinamide ring at the left-hand side.

tide-binding fold, or Rossmann fold, found in many soluble dehydrogenases [33,34]. Thus, *rr*dIII contains an open, twisted β-sheet of six parallel strands (β1 to β6). Looking across the β-sheet, the strands appear in the order β3-2-1-4-5-6, and they are flanked by helices or loops (A to F). The two βαβαβ motifs (β1-β3 and β4-β6) are linked by a 'cross-over' helix (C) between the C-terminus of strand β3 and the N-terminus of β4. Helices A, B and F lie on one side of the β-sheet, whilst helix C, helix D/loop D and loop E are on the opposite side. Helix D/loop D forms an extended structure which protrudes from the sheet. Loop E passes over loop D (see Fig. 4) and the nucleotide-binding site. The N-terminal 28 amino acids of *rr*dIII are largely unstructured, with few inter-residue NOEs. Residues 29–35 curl around the protein, with Val31-Ala33 forming a short, extended strand, which lies parallel to β6. This is linked to β1 by an additional helix, designated helix 0, which lies on the same face of the β-sheet as helices A, B and F. The overall fold of *rr*dIII, determined by NMR methods, is remarkably similar to those revealed in the X-ray structures of the equivalent proteins derived from mammalian sources, notably human dIII (*hs*dIII [1,14]) and bovine dIII (*bt*dIII) [13]. In view of these similarities, the perceived differences between the crystal structures of *hs*dIII and *bt*dIII, and the preliminary 'global fold' of *ec*dIII [16], might simply result from an insufficient number of NOEs used to model the *E. coli* protein. The solution and crystal structures share similar conformations in their more unusual features, such as helix D/loop D and loop E; these might play an important role in the function of the protein (see below).

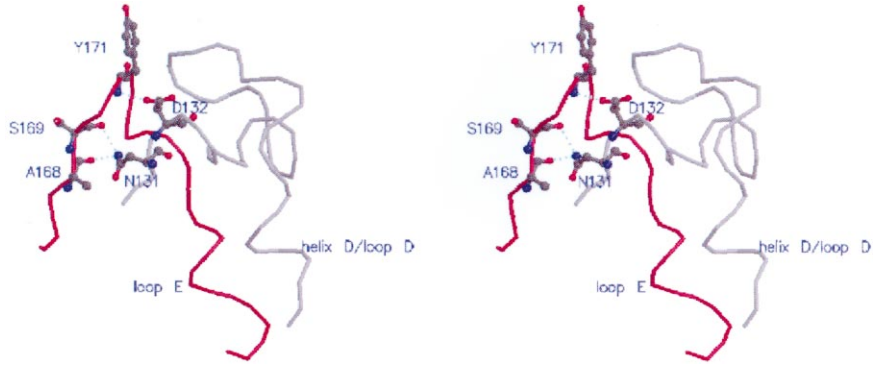

Fig. 4. Structure of helix D/loop D and loop E. The stereo view depicts the backbone C^{α} trace of the averaged structure, for residues Gly129-Gly158 (helix D/loop D) in grey, and Arg165-Asn183 (loop E) in red. Residues Asn131, Asp132, Ala168, Ser169 and Tyr171 are shown in ball-and-stick representation, along with the predicted hydrogen bonds between them (turquoise, dotted lines).

3.3. The unusual mode of nucleotide binding in transhydrogenase dIII

In the classical Rossmann fold, the dinucleotide is bound in a groove across the C-termini of the β-strands. In the case of NAD(P)(H)-binding proteins, the adenosine moiety lies in a cleft between strands β1 and β2, and the pyrophosphate group contacts the loop connecting β1 and helix A. This loop contains the Gly-X-Gly-X-X-Gly (NAD(H)-binding) or Gly-X-Gly-X-X-Ala/Val (NADP(H)-binding) 'fingerprint' sequence [35]. In several NADP(H)-binding proteins, one or more positively charged residues are located near the C-terminal end of β2, and interact with the 2′-phosphate of the adenosyl ribose [36]. All known transhydrogenase sequences contain the NADP(H) fingerprint (residues Gly54-Val59 of *rr*dIII), and an invariant pair of basic residues (His85, Arg90 in *rr*dIII). It was therefore predicted that $NADP^+$ would be bound to *E. coli* dIII in the conventional manner [37].

A list of contacts between *rr*dIII and the bound $NADP^+$, derived mainly from the NOE data, is given in Table 2. Intra-nucleotide NOEs show that the nicotinamide ring is *syn* with respect to its sugar, while the adenosine is in the *anti* configuration. Surprisingly, however, the adenosine lies over the C-termini of strands β4 and β5, and the nicotinamide lies over the C-terminus of strand β2, protruding out into the solvent above the short β3. Although there are relatively few NOEs between the protein and the nicotinamide ring, the identified contacts provide very adequate constraints for the ribose rings and the adenine, and allow us to be confident of this unusual orientation of the bound nucleotide, which is the opposite to that found in other NAD(P)(H)-binding proteins. The same result was obtained in the crystal structures of the mammalian dIII proteins [1,13,14].

As in the classical Rossmann fold, the fingerprint sequence of *rr*dIII is located at the C-terminus of strand β1. However, due to the reversed orientation of the $NADP^+$, the backbone amide groups of this sequence do not make the extensive contacts with the pyrophosphate seen in the classical binding mode. The first glycine (Gly54) of the fingerprint, which would normally form a sharp bend, instead adopts an extended conformation within strand β1. The bend away from the strand occurs at the next residue, Tyr55. The aromatic ring of this residue, which is also invariant in known dIII sequences, points outwards from the protein, and is probably involved in hydrophobic interactions with the adenosine, while its backbone amide lies within H-bonding distance of the nucleotide pyrophosphate. The second glycine (Gly56) allows close approach of the adenosine, rather than the pyrophosphate. As a consequence of the novel orientation of the nucleotide, the invariant His85 and Arg90, contrary to the prediction of [37], do not lie close to the 2′-phosphate of the adenosyl ribose.

The most important region of *rr*dIII for binding the nucleotide pyrophosphate lies at the C-terminus of strand β4. Residues in this region of the protein have an equivalent role to those at the C-terminus of strand β1 in the classical Rossmann fold. An invariant glycine (Gly129) allows a 90° bend in the poly-

Table 2
Proton connectivities between *rr*dIII and bound $NADP^+$

dIII residue protons		$NADP^+$ atoms
(A) NOEs		
Tyr55	HD+, HE+	adenine H8
Val59	HG2+	adenine H8
Ala60	HB+	adenine H2
Val87	HA	nicotinamide H7+
	HB	nicotinamide H2
	HG1+, HG2+	nicotinamide H2, nicotinamide ribose H2
Ala88	HA	nicotinamide ribose H2, H5+
Arg90	HA	nicotinamide H7+
Gly129	HA1, HA2	adenosyl ribose H1
Val133	HG2+	nicotinamide ribose H5+, H4, H3
Ile163	HG2+	adenine H2
Lys164	HA	adenine H2, adenosyl ribose H1
	HB+	adenosyl ribose H1
Gly170	HA2	adenosyl ribose H5″
Tyr171	HD+, HE+	nicotinamide ribose H1
Ala191	HA, HB+	adenine H2
(B) Hydrogen bonds		
Val133	HN	nicotinamide O1
Lys164	HZ+	adenosyl 2′-phosphate (OP+)

X-PLOR atom nomenclature is used. The NOEs were divided into two classes on the basis of their intensities. All but three were weak, and the upper limit of each of these restraints was set to 5 Å. The upper distance limit of the three stronger NOEs (Val133 HG2+/nicotinamide ribose H3; Gly170 HA2/adenosyl ribose H5″; and Ala191 HB+/adenine H2) was set to 3.5 Å.

peptide backbone, and displays NOEs to the adenosyl ribose. The backbone amide groups of Asn131, Asp132 and Val133 are all potential H-bond donors to the pyrophosphate. Although amide protons involved in intra-protein H-bonding are not expected to exchange rapidly with solvent, the protons from these residues, except Val133, exchanged $>90\%$ within 5 h [15]. This may be a consequence of the exchange of bound nucleotide with that in the buffer ($k_{off} = 0.03\ s^{-1}$ [5]) allowing the amide groups to be exposed to solvent for short periods. The invariant Asn131 fulfils the role of the second glycine in the classical fingerprint, allowing the close approach of the pyrophosphate to the protein backbone. The counterpart of the Val/Ala of the NADP(H) fingerprint is less conserved (Thr134 in *rr*dIII), and has no obvious role in nucleotide binding. In proteins where NAD(P)(H) is bound in the conventional orientation, the pyrophosphate lies over the N-terminus of helix A, but in *rr*dIII, the pyrophosphate is positioned over the N-terminus of the helix D/loop D structure.

One lysyl ε-NH_3^+ group was assigned from the ^{15}N-resolved NOESY spectrum to Lys164. The proton signals from such groups are not usually observed, due to fast exchange with solvent. A likely explanation is that Lys164 forms an H-bond with the 2′-phosphate of the adenosyl ribose. The side chain of the adjacent Arg165 might also interact with the 2′-phosphate, but it has not been fully assigned and is therefore not well constrained in the solution structure. These residues might be responsible for the NADP(H)-binding specificity of the protein.

The adenine ring of the nucleotide is well constrained by NOEs to the side chains of residues on both sides of its binding pocket. By contrast, the nicotinamide ring exhibits NOEs only from the *pro-S* face (to Val87). Access to the *pro-R* face is, however, obstructed by the backbone of residues Gly89-Met91. The structure in this region is thus consistent with the stereospecificity of hydride transfer in the complete enzyme, to and from the more exposed *pro-S* side of NADP(H) [38].

Two tyrosine residues, Tyr55 and Tyr171, lie on either edge of the binding cleft. Tyr55 is invariant, while Tyr171 is strongly conserved (Tyr/Phe). In the crystal structure of *hs*dIII, the corresponding Tyr residues, along with the equivalent of Arg90 in *rr*dIII, form a cluster over the pyrophosphate, which may serve to prevent nucleotide release. Although the side chain of Arg90 is less constrained by NOEs, a similar clustering of residues may occur in *rr*dIII. In the family of NMR structures, Tyr55 lies within 4–5 Å of the adenine ring and Tyr171 is approx. 5–6 Å from the nicotinamide ring. NOEs were detected between the Tyr55 ring and the adenosyl H8 proton, and between the Tyr171 ring and the nicotinamide ribose H1′ proton (Table 2). It is therefore possible that the two rings participate in stacking interactions with the respective nucleotide rings. We previously measured changes in magnetic environment of the amide groups of *rr*dIII upon replacing bound $NADP^+$ with NADPH [15]. The magnetic effects correspond to a conformational change during the hydride transfer step. The residues most affected were located in the vicinity of the nucleotide binding site (including Tyr55 and Tyr171), in helix D/loop D, and in loop E. A stacking interaction between Tyr171 and the nicotinamide ring could provide a mechanism for the protein to distinguish between bound $NADP^+$ and NADPH. Following oxidation or reduction of the bound nucleotide, a change in the orientation of Tyr171 resulting from altered stacking could produce conformational changes in helix D/loop D and loop E, which in turn might be transmitted to dII via interactions with its surface-exposed loops (see below).

3.4. Interactions between dIII and dI

Direct hydride transfer between NAD(H) and NADP(H) requires that the C4 atoms of the two nicotinamide rings must come close to each other [11]. Experiments were performed to investigate the effect on the magnetic environment of the amide groups of *rr*dIII upon binding of *rr*dI [15]. Eight residues that showed preferential broadening are clustered around the β3 edge of the β-sheet, suggesting that this region forms at least part of the dI binding site on dIII (Fig. 5). In a model of *rr*dI based on the crystal structure of alanine dehydrogenase [39], the dihydronicotinamide ring of NADH is located in a cleft [40]. It is proposed that the ridge-like region of dIII bearing the nicotinamide ring of $NADP^+$ inserts into the cleft of dI to bring the two nicotinamide C4 atoms into apposition.

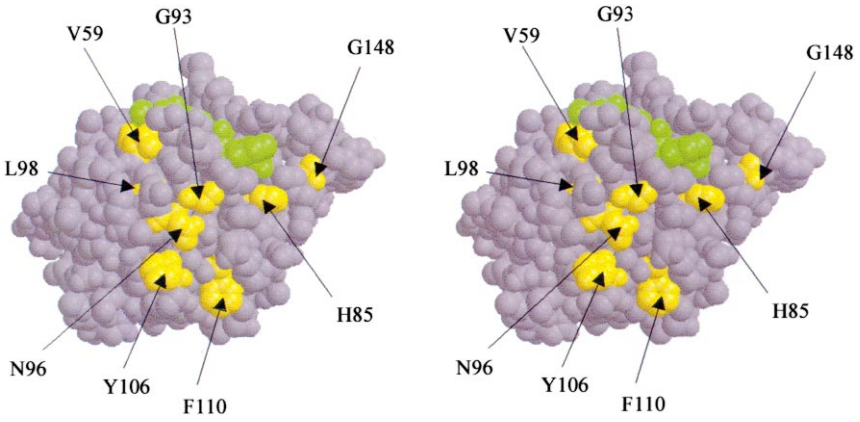

Fig. 5. Stereo view of the proposed dI:dIII binding surface. A Van der Waals model of residues 29–203 of *rr*dIII is presented. Bound $NADP^+$ is shown in green, with the nicotinamide ring to the right. The eight residues whose backbone amides broaden upon addition of dI [15] are shown in yellow. Helix D/loop D protrudes from the right-hand side of the molecule.

3.5. Interactions between dIII and dII

The face of *rr*dIII comprising helices 0, A, and F is polar, with few conserved residues, and is likely to be exposed to the solvent in intact transhydrogenase. The opposite side of the protein, including helix C, helix D/loop D and loop E, is more hydrophobic and has more conserved residues, including a conserved acidic patch. It therefore seems a better candidate to contain the sites of interaction of dIII with dI and dII. Given the likelihood that dI interacts with the β3 end of the β-sheet (see above), we suggest that surface loops of dII might interact with parts of helix D/loop D and loop E.

In isolated dIII, loop E lies over the pyrophosphate of the bound $NADP^+$ (Figs. 3 and 4). Nucleotide release is extremely slow, and we have suggested that this conformation of dIII corresponds to an 'occluded' state of the intact enzyme [1,14]. The occluded state catalyses rapid hydride transfer between dI and dIII, without coupling to proton translocation [41]. During the catalytic cycle, the intact enzyme probably undergoes conformational changes between the occluded state and an 'open' state, from which nucleotide can readily dissociate. Such a conformational change is likely to involve loop E and the neighbouring helix D/loop D, and could be linked to the proton translocation process by the interaction of these structures with surface loops of dII. There are possible hydrogen bonds between residues of helix D/loop D and loop E: Asn131 side chain amide to backbone carbonyls of Ala168 and Ser169, and Tyr171 amide to Asp132 side chain carboxylate.

A key role in controlling the binding and release of NADP(H) is likely to be performed by the invariant acidic residue, Asp132, located in helix D/loop D (Fig. 4). Asp132 is positioned immediately below the pyrophosphate of the bound NADP(H), an unexpected place to find an acidic residue. Its side chain carboxylate is a potential hydrogen-bond acceptor from the amide of Tyr171 in the *rr*dIII solution structure, and a corresponding interaction is seen in the *hs*dIII crystal structure. Solvent access to Asp132 is severely restricted by the ring of Tyr171, the bound nucleotide, and other residues of helix D/loop D and loop E. We therefore suggest that the side chain of Asp132 might have a raised pK_a in this conformation of the enzyme, and that protonation and deprotonation of Asp132 during the catalytic cycle might be associated with the transition between occluded and open states of dIII. Site-directed mutagenesis on the equivalent aspartate residue of the intact *E. coli* enzyme (βAsp392) led to severely inhibited transhydrogenation [42,43]. Interestingly, the complex between expressed βAsp392Cys *ec*dIII and *rr*dI catalysed 'reverse' transhydrogenation ten times faster than wild-type *ec*dIII:*rr*dI [37]. This suggests that the nucleotide dissociates more readily from the mutant.

There are two possibilities for coupling the protonation and deprotonation of Asp132 with the translocation of protons through dII. First, the protons from dII might enter dIII, in the vicinity of helix D/loop D and loop E, and bind directly to the aspar-

tate. Second, changes in the ionisation state of Asp132 might arise indirectly, as a result of a conformational change propagated from dII through helix D/loop D and loop E. At present there is no biochemical evidence to favour one mechanism over the other, but we suggest that protonation and deprotonation events, however they are accomplished, play an essential role in controlling the rate of product release from dIII.

Acknowledgements

We thank Scott White, Jamie Venning, and Sarah Peake for valuable discussions, and Tony Pemberton for maintenance of the NMR facility. We thank the Biotechnology and Biological Sciences Research Council and the Wellcome Trust for financial support. We also acknowledge the use of computing facilities funded by bioinformatics infrastructure grant G.4600017 from the Medical Research Council to the University of Birmingham.

References

[1] J.B. Jackson, S.J. Peake, S.A. White, FEBS Lett. 464 (1999) 1–8.
[2] G. Ambartsoumian, R. Dari, R.T. Lin, E.B. Newman, Microbiology 140 (1994) 1737–1744.
[3] L.A. Sazanov, J.B. Jackson, FEBS Lett. 344 (1994) 109–116.
[4] C. Diggle, M. Hutton, G.R. Jones, C.M. Thomas, J.B. Jackson, Eur. J. Biochem. 228 (1995) 719–726.
[5] C. Diggle, T. Bizouarn, N.P.J. Cotton, J.B. Jackson, Eur. J. Biochem. 241 (1996) 162–170.
[6] O. Fjellström, C. Johansson, J. Rydström, Biochemistry 36 (1997) 11331–11341.
[7] M. Yamaguchi, Y. Hatefi, J. Biol. Chem. 270 (1995) 28165–28168.
[8] S.J. Peake, J.D. Venning, J.B. Jackson, Biochim. Biophys. Acta 1411 (1999) 159–169.
[9] M. Hutton, J.M. Day, T. Bizouarn, J.B. Jackson, Eur. J. Biochem. 219 (1994) 1041–1051.
[10] Y. Hatefi, M. Yamaguchi, FASEB J. 10 (1996) 444–452.
[11] J.D. Venning, R.L. Grimley, T. Bizouarn, N.P.J. Cotton, J.B. Jackson, J. Biol. Chem. 272 (1997) 27535–27538.
[12] J.D. Venning, J.B. Jackson, Biochem. J. 341 (1999) 329–337.
[13] G.S. Prasad, V. Sridhar, M. Yamaguchi, Y. Hatefi, C.D. Stout, Nat. Struct. Biol. 6 (1999) 1126–1131.
[14] S.A. White, S.J. Peake, S. McSweeney, G. Leonard, N.P.J. Cotton, J.B. Jackson, Structure 8 (2000) 1–12.
[15] P.G. Quirk, M. Jeeves, N.P.J. Cotton, K.J. Smith, J.B. Jackson, FEBS Lett. 446 (1999) 127–132.
[16] C. Johansson, A. Bergqvist, O. Fjellström, J. Rydström, B.G. Karlsson, FEBS Lett. 458 (1999) 180–184.
[17] M. Jeeves, K.J. Smith, P.G. Quirk, N.P.J. Cotton, J.B. Jackson, J. Biomol. NMR 13 (1999) 305–306.
[18] A. Bax, G.W. Vuister, S. Grzesiek, F. Delaglio, A.C. Wang, R. Tschudin, G. Zhu, Methods Enzymol. 239 (1994) 79–105.
[19] L.E. Kay, G.Y. Xu, A.U. Singer, D.R. Muhandiram, J.D. Forman-kay, J. Magn. Reson. B 101 (1993) 333–337.
[20] K. Gehring, I. Ekiel, J. Magn. Reson. 135 (1998) 185–193.
[21] S. Grzesiek, H. Kuboniwa, A.P. Hinck, A. Bax, J. Am. Chem. Soc. 117 (1995) 5312–5315.
[22] M. Rance, O.W. Sorenson, G. Bodenhausen, G. Wagner, R.R. Ernst, Biochem. Biophys. Res. Commun. 117 (1983) 479–485.
[23] C. Zwahlen, P. Legault, S.J.F. Vincent, J. Greenblatt, R. Konrat, L.E. Kay, J. Am. Chem. Soc. 119 (1997) 6711–6721.
[24] J.S. Hu, A. Bax, J. Biomol. NMR 9 (1997) 323–328.
[25] O.W. Zhang, L.E. Kay, J.P. Olivier, J.D. Forman-kay, J. Biomol. NMR 4 (1994) 845–858.
[26] M. Gueron, P. Plateau, M. Decorps, Prog. Nucl. Magn. Reson. Spect. 23 (1991) 135–209.
[27] G.W. Vuister, G.M. Clore, A.M. Gronenborn, R. Powers, D.S. Garrett, R. Tschudin, A. Bax, J. Magn. Reson. B 101 (1993) 210–213.
[28] D.R. Muhandiram, G.Y. Xu, L.E. Kay, J. Biomol. NMR 3 (1993) 463–470.
[29] M. Nilges, S.I. O'Donoghue, Prog. Nucl. Mag. Reson. Spect. 32 (1998) 107–139.
[30] A.T. Brünger, X-PLOR Version 3.851, Yale University Press, New Haven, CT, 1996.
[31] R.A. Laskowski, J.A.C. Rullmann, M.W. MacArthur, R. Kaptein, J.M. Thornton, J. Biomol. NMR 8 (1996) 477–486.
[32] P.J. Kraulis, J. Appl. Cryst. 24 (1991) 946–950.
[33] W. Eventoff, M.G. Rossmann, CRC Crit. Rev. Biochem. 3 (1975) 111–140.
[34] C.R. Bellamacina, FASEB J. 10 (1996) 1257–1269.
[35] R.K. Wierenga, P. Terpstra, W.G.J. Hol, J. Mol. Biol. 187 (1986) 101–107.
[36] N.S. Scrutton, A. Berry, R.N. Perham, Nature 343 (1990) 38–43.
[37] O. Fjellström, M. Axelsson, T. Bizouarn, X. Hu, C. Johansson, J. Meuller, J. Rydström, J. Biol. Chem. 274 (1999) 6350–6359.
[38] R.R. Fisher, R.J. Guillory, J. Biol. Chem. 246 (1971) 4687–4693.
[39] P.J. Baker, Y. Sawa, H. Shibata, S.E. Sedelnikova, D.W. Rice, Nat. Struct. Biol. 5 (1998) 561–567.
[40] P.G. Quirk, K.J. Smith, C.M. Thomas, J.B. Jackson, Biochim. Biophys. Acta 1412 (1999) 139–148.
[41] T. Bizouarn, S. Stilwell, J. Venning, N.P.J. Cotton, J.B. Jackson, Biochim. Biophys. Acta 1322 (1997) 19–32.
[42] J. Mueller, X. Hu, C. Bunthof, T. Olausson, J. Rydström, Biochim. Biophys. Acta 1273 (1996) 191–194.
[43] X. Hu, J. Zhang, O. Fjellström, T. Bizouarn, J. Rydström, Biochemistry 38 (1999) 1652–1658.